AN ABSTRACT OF THE THESIS OF

Mahbub I. Ahmed for the degree of Master of Science in Electrical and Computer Engineering presented on November 29,1990.

Title: Performance Analysis of Least Square Error $|\omega|$ Filter for Image Reconstruction from Projection.

Redacted for privacy

Abstract approved: _____
R. C. Rathja

A study has been made of least square error $|\omega|$ filters for image reconstruction from projection. Only parallel beam projection has been considered for image reconstruction.

Although the Convolution Backprojection method tends to generate the best reconstructed images, the computational overhead of this method is very large. Use of short length filters can speed up the convolution process.

Two kinds of short filters have been investigated in this study. Least square error filters are designed using rectangular windows. These filters are reported to have limited success in the case of divergent beam reconstruction. This study investigates the performance of truncated least square error $|\omega|$ filters for parallel beam image reconstruction.

Use of weighted least square error $\left|\frac{2}{a}\,\mathrm{Sin}\frac{\omega a}{2}\right|$ filters has already been reported for reconstructing images. Performance of weighted least square error $|\omega|$ filters has been studied in this work. A comparison of the performance of the two filter types is included.

Performance Analysis of Least Square Error $|\omega|$ Filter for Image Reconstruction from Projection

by

Mahbub I. Ahmed

A THESIS

submitted to

Oregon State University

in partial fulfillment of
the requirements for the
degree of

Master of Science

Completed November 29, 1990

Commencement June 1991

APPROVED:

Redacted for privacy

Associate Professor of Electrical and Computer Engineering in charge of major

Redacted for privacy

Head of Department of Electrical and Computer Engineering.

Redacted for privacy

Dean of Graduate School

Date thesis is presented November 29, 1990

Typed by Mahbub I. Ahmed for Mahbub I. Ahmed

TABLE OF CONTENTS

LIST OF FIGURES

PERFORMANCE ANALYSIS OF LEAST SQUARE ERROR $|\omega|$ FILTER FOR IMAGE RECONSTRUCTION FROM PROJECTION

CHAPTER I

INTRODUCTION

Introduction: Digital reconstruction of an image from its projection has become an important subject of research during the past few years. This problem has arisen independently and repeatedly in various scientific, medical and technical fields. The range of applicability is diversified. The nonmedical areas where such techniques are used include radio-astronomy, optical interferometry, electron microscopy, and geophysical exploration. In the area of medical imaging, which most probably has received the greatest contribution from this technique, multiple projection data generated by x-ray are used to reconstruct the internal structure of the human body. This process is called *Computerized Tomography.* Other medical applications include ultrasonic imaging and nuclear medicine. The aim of this technique in ultrasonic imaging is similar to that in x-ray imaging but the problem is made more difficult by the refraction of the ultrasound as it propagates through tissue. In nuclear medicine, the aim is to reconstruct the distribution of the concentration of a gamma-ray emitting isotope in a given cross section of the body.

Because of its diversified applications, the problem of image reconstruction from projection has been repeatedly considered by researchers, resulting in the development of various algorithms for this purpose. Different algorithms work favorably under different conditions. Speed of such algorithms is an important issue and this thesis deals with the improvement of speed for a class of algorithm in this area for a specific type of implementation.

Motivation and Objective: Among the available image reconstruction techniques from projections, the *Convolution Backprojection* [10] method tends to generate the best quality images. There are two steps involved in this method. In the first step, projection data are measured for a particular orientation of rays and they are convolved with the impulse response of a filter whose frequency response approximates $|\omega|$ within the frequency range of interest. The result of this convolution is a *Modified Projection*, denoted as $Q(t)$. This process is repeated for all projections measured from different angles and a set of modified projections $[Q_0(t), Q_1(t), Q_2(t) \ldots Q_{n-1}(t)]$ is generated, where n is the total number of projections.

In the second step, the contribution of each of the modified projection $Q_i(t)$ to a particular pixel is calculated and they are added together to find the reconstructed value of that pixel. That is, if Ci represents the contribution of $Q_i(t)$ for a pixel at the point (x_0,y_0), then the reconstructed pixel value at that point is $f(x_0,y_0) = [\, C_0 + C_1 + \ldots + C_{n-1} \,]$. This process is repeated for all the pixels of the image.

Since a projection is of finite duration, it has a finite number of non-zero samples. If the total number of samples in each projection is K, then K samples in each of the modified projections are sufficient to reconstruct the image. To calculate a sample of a modified projection, K multiplications are needed; and for K samples of a modified projection, the required number of multiplication is K^2. Assuming that the number of multiplications required for backprojecting a single point is 4 [1], $4N^2$ additional multiplications are needed; where N x N is the image size. This gives that for n projections, approximately $n(K^2 + 4N^2)$ operations are required. In most cases K = N, and assuming that n is also in the same order of K and N, it can be said that the total number of multiplications is in the order of N^3. Although the Convolution Backprojection method tends to give the best quality reconstructions, it is a slow process.

Improvement of the speed of the Convolution Backprojection method has been the interest of different research work. Some of the work concentrates on improving the speed of the convolution part [2] and some deals with the backprojection part [3]. The speed of backprojection depends upon the type of interpolation used but there is always a tradeoff between the quality of the reconstruction and the speed of the algorithm used. This tradeoff is made depending upon the application. Although exact interpolation can result in a better reconstruction of an image, Shepp and Logan [1] have shown that the simulated cross section of a brain phantom can be reconstructed within acceptable accuracy by using linear interpolation. Kwoh et. al. [3] have demonstrated that it is possible to reconstruct the image of

a circular symmetric phantom by zero order interpolation while maintaining accuracy acceptable for many practical applications.

The problem of speed improvement of the convolution process has also been considered from different angles. When the size of data is very large for a projection, use of FFT methods can give considerable saving compared to direct convolution suggested by Shepp and Logan [1]. Finite field transforms have been used in different applications [4] to improve the speed of the convolution. The amount of computation required to perform the convolution may also be reduced by approximating the impulse response of the required filter by a function which is piecewise constant over intervals several times larger than the sampling interval [2]. The implementation of multiplications with reduced precision has also been found to improve the speed of the algorithm at the expense of some accuracy [2].

Another speed improvement technique for Convolution Backprojection is the use of truncated filters. Edelheit et. al [5] have suggested the use of rectangular windows for truncating the filter, where the width of the window is less than (2K-1); K being the number of samples in a projection. This method has been proposed for reconstructions from divergent beam X-rays. Lewitt et. al [6] have suggested the use of weighted least square filters to improve the result. They have tested their method for approximating Shepp and Logan's filter response which performs well under noisy conditions.

The idea of speed improvement of the convolution backprojection method motivates this research work because of its potential impact on practical applications. Of course there is always a tradeoff between the quality of the reconstructed images and the speed, but that is always decided by the requirements of a specific application. Truncated filters improve the speed of software and may be implemented in hardware for further improvements. Ramachandran's filter [7] performs better for reconstructing high frequency components and the motivation of this work is to approximate this filter's frequency response by short length filters and study their performance.

Statement of the Problem: It has been stated that the Convolution Backprojection method tends to give better reconstructions among the other available techniques. For an N x N image, the number of computational operations required for this method is in the order of N^3. This computational complexity causes the process to be slow and this thesis deals with the development of a speed improvement scheme for this algorithm.

The objective of this thesis is to apply rectangular window and weighted least square error filters for approximating the frequency response of $|\omega|$ and to evaluate their performances by producing simulation results. Only reconstruction from parallel beams have been considered.

Thesis Organization: This thesis has been divided into five different chapters. Each chapter deals with different issue of image reconstruction. Descriptions of different chapters are given below.

Chapter II gives an overview of different reconstruction techniques. It describes the Projection Slice theorem, which is the backbone of many reconstruction techniques, in detail. Three major reconstruction techniques, namely Direct Fourier Technique, Algebraic Reconstruction Technique and the Convolution Backprojection Method have been discussed here.

Chapter III discusses the use of truncated $|\omega|$ filters for image reconstruction from projections with the Convolution Backprojection method. It discusses the nature of the error present in both the least square and weighted least square error filters.

Chapter IV deals with simulation results. A simulated brain phantom has been reconstructed by least square and weighted least square $|\omega|$ filters. Discussions about the results have also been included in this chapter.

Finally in chapter V, the author summarizes his contributions in this thesis and discusses the conclusions derived. Recommendations for further work are also presented.

CHAPTER II

OVERVIEW OF RECONSTRUCTION TECHNIQUES

Introduction: There are many algorithms available for image reconstruction from projections. The literature review reveals that they can be placed in three major classes:

1) Direct Fourier Technique
2) Algebraic Reconstruction Technique, and
3) Convolution Backprojection Method.

Other approaches exist, but they are variations of these techniques.

This thesis is mainly involved with the Convolution Backprojection method. Discussions about various aspects of this technique are presented throughout the thesis in different contexts. In this chapter a brief discussion about each technique is presented. Before discussing any individual technique, it is important to introduce the basic theorem behind the development of these algorithms, which is commonly known as the *Projection Slice Theorem.*

Projection Slice Theorem: Assume f(x,y) is the object density function at the point (x,y) and $F(\omega_x,\omega_y)$ is its two dimensional Fourier transform, the Projection Slice theorem can be stated as [8]:

The Fourier transform of the projection at orientation θ is a section (line sampling) of the Fourier transform of f(x,y), where the sampling line passes through the origin $\omega_x = \omega_y = 0$ and makes an angle θ with the ω_x axis.

Projection can be defined as a shadowgram obtained by illuminating an object by penetrating radiation. An illustration is shown in Figure 2.1. If a ray is passing through an object, it gets attenuated at every point depending upon the density of the object at that point. So the measured projection at a point is proportional to the total attenuation of the ray incident on that point.

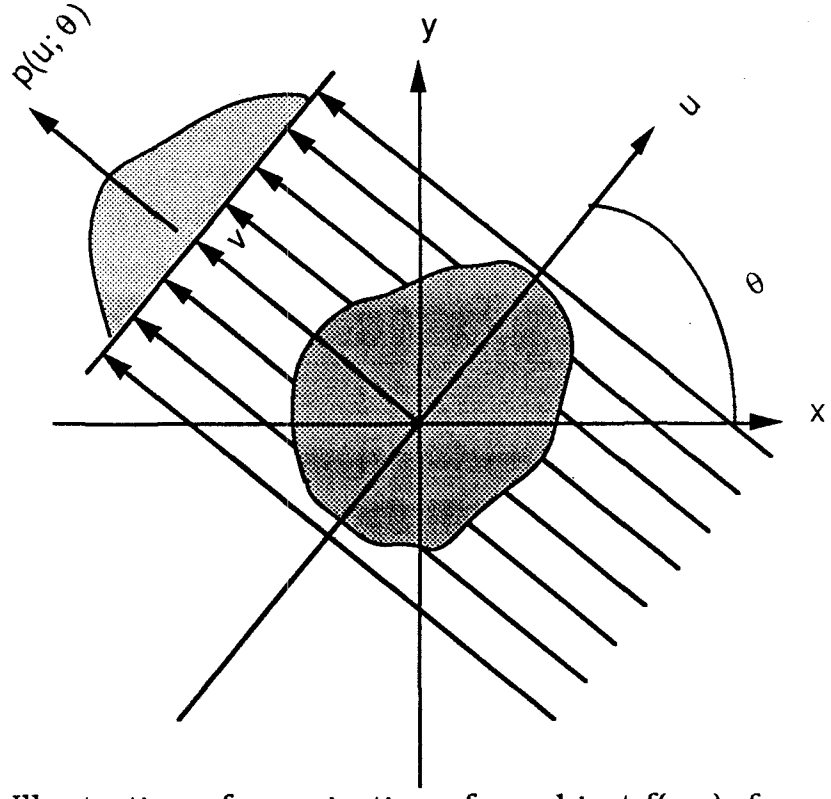

Fig 2.1: Illustration of a projection of an object f(x,y) for an orientation of angle θ .

Refering to Figure 2.1, an object f(x,y) is placed on the x-y coordinate system. Projection data are generated by passing a set of parallel rays at orientation θ. Orientation θ means that the line drawn perpendicular to the set of rays and passing through the origin of x-y co-ordinates makes an angle θ with the x axis.

For a particular orientation, θ is a constant and the measured projection p(u;θ) at a distance u from the origin of the u-v coordinates is a one dimensional function. Since the measured projection is proportional to the total attenuation of a ray as it passes through the object and the attenuation is again proportional to the density of the object at that point, mathematically we can write that the projection measured at a distance t from the origin of the u-v domain is:

$$p(t\ ;\ \theta) = \int_{L(t,\theta)} f(x,y)\ dv \qquad [2.1]$$

where $L(t,\theta)$ means that the function has been integrated along the line $x\cos\theta+y\sin\theta = t$. Expressing Equation [2.1] in a general form as a function of u and v, it can be written as

$$p(u\ ;\ \theta) = \int_{-\infty}^{\infty} f(\ u\cos\theta - v\sin\theta\ ,\ u\sin\theta + v\cos\theta)\ dv \qquad [2.2]$$

Let $P(\omega;\theta)$ denotes the one dimensional Fourier transform of $p(u;\theta)$ with respect to the variable u. That gives,

$$P(\omega;\theta)=\int_{-\infty}^{\infty} p(u\ ;\ \theta)\ e^{-j\omega u}\ du \qquad [2.3]$$

Now, the two dimensional Fourier transform $F(\omega,\theta)$ of the object density function f(x,y) is given in the polar co-ordinates as

$$F(\omega,\theta)=\int_{-\infty}^{\infty}\int_{-\infty}^{\infty} f(x,y)\ e^{-j(x\omega\cos\theta+y\omega\sin\theta)}\ dx\ dy \qquad [2.4]$$

If the items in Equation [2.4] are expressed as a function of u and v, which is a rotated co-ordinate system with respect to the x-y domain, x and y are replaced by

$$x = u\cos\theta - v\sin\theta$$
$$y = u\sin\theta + v\cos\theta \qquad [2.5]$$

and

$$F(\omega,\theta) = \int_{-\infty}^{\infty}\int_{-\infty}^{\infty} f(u\cos\theta - v\sin\theta\ ,\ u\sin\theta + v\cos\theta)\ e^{-ju\omega}\ du dv$$

$$= \int_{-\infty}^{\infty}\left\{\int_{-\infty}^{\infty} f(u\cos\theta - v\sin\theta\ ,\ u\sin\theta + v\cos\theta)\ dv\right\} e^{-ju\omega}\ du$$

$$= \int_{-\infty}^{\infty} p(u\ ,\ \theta)\ e^{-ju\omega}\ du$$

$$= P(\omega\ ;\ \theta) \qquad [2.6]$$

Equation [2.6] verifies the statements of the Projection Slice Theorem.

It follows from the above development, that if projections are measured from different angles for a number of orientations θ, then it is equivalent to the knowledge of the Fourier transform of the object function on a star shaped region on the Fourier plane. This is the basis of many reconstruction techniques and in the following sections the development of various classes of algorithms are discussed.

Direct Fourier Technique: The Direct Fourier Techniques for reconstructing an image from its projection consists of three steps:

1) Computation of the line samples of the Fourier transform of the object function f(x,y) from the measurements of the projections.
2) Generation of the samples of the Fourier transform $F(\omega_x,\omega_y)$ of the object f(x,y) on a rectilinear grid by interpolating the known polar grid; and
3) Computation of the inverse two dimensional Fourier transform of the rectilinear grid to evaluate the approximate object function f(x,y).

The line samples of the Fourier transform of the object are computed by taking the one dimensional Fourier transform of the projection data. By the Projection Slice theorem, if a projection is measured for the orientation of an angle θ and then the one dimensional Fourier transform of that data is calculated, it is equivalent to the knowledge of the values of the two dimensional Fourier transform of the object along the line which passes through the origin $\omega_x = \omega_y = 0$ and makes an angle θ with the ω_x axis. i.e.

$$F(\omega ; \theta) = \int p(u ; \theta)\, e^{-j\omega u}\, du$$

Refering to Figure 2.2, it can be said that if a projection is taken at θ_1 orientation and another in θ_2 orientation, the values of the

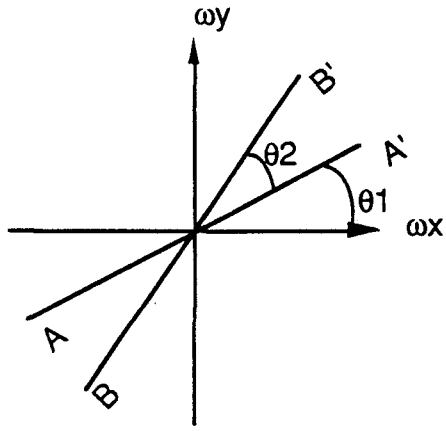

Fig 2.2: Line samples in the Fourier space of an object function f(x,y)

Fourier transform $F(\omega_x,\omega_y)$ of the object f(x,y) can be generated along the lines AA' and BB'. Similarly if projections are measured for a set of orientations $[\theta_0, \theta_1, \theta_2, \ldots\ldots\ldots, \theta_{n-1}]$, for any initial angle θ_0 and $(\theta_{i+1} - \theta_i) = (\pi + \theta_0)/n$, it is possible to genarate a star shaped sample space of the function $F(\omega_x,\omega_y)$ as shown in Figure 2.3a. Since in all practical applications the samples of the projections will be measured, equispaced samples of the Fourier transform of the projection data will be calculated along each radial line and the resulting situation is shown in Figure 2.3b. This figure shows that samples of the Fourier transform are on a polar grid. For a particular θ, the samples of the Fourier transform $F(k,\theta)$ along the radial line can be calculated as

$$F(k,\theta) = \sum_{n=-N/2}^{N/2} p(n;\theta)\, e^{-j\frac{2\pi}{N+1}nk} \qquad [2.7]$$

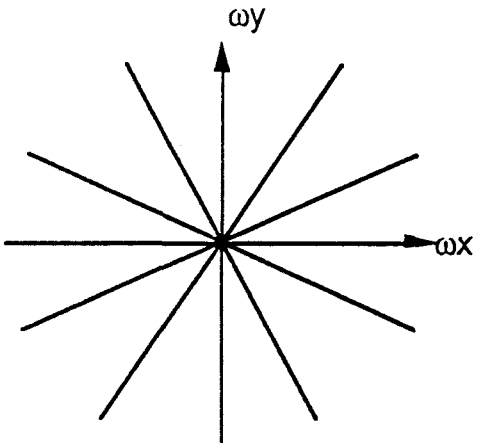

Fig 2.3a: Star shaped line sampled Fourier space.

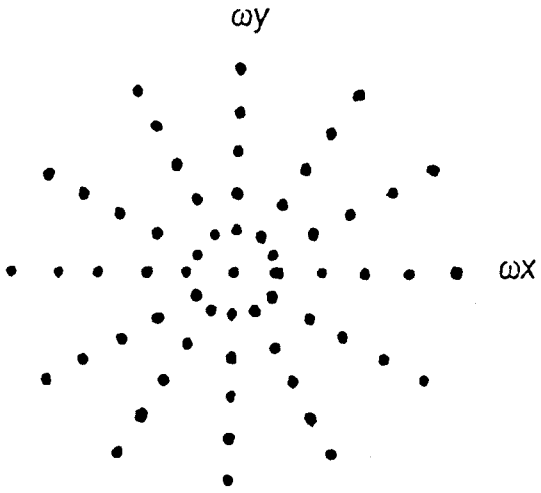

Fig 2.3b: Sample points on a polar grid of the Fourier space.

Different interpolation schemes are used for the second step of this technique. Two of the simplest kinds are nearest neighbor estimation and bilinear interpolation [8]. The resulting sample grid is shown in Figure 2.4.

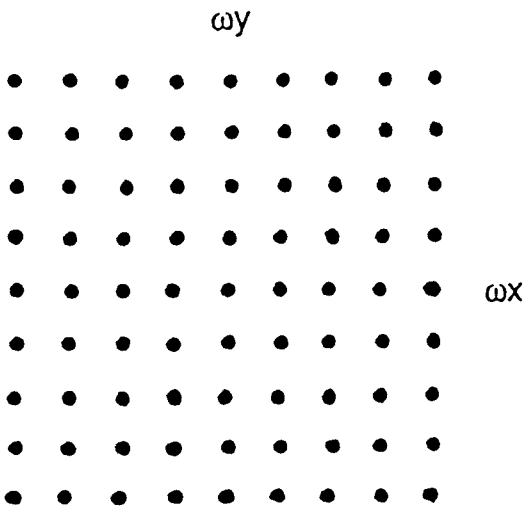

Fig 2.4: Sample points on a rectangular grid of the Fourier space.

The two dimensional inverse Fourier transform of these samples generates the object data.

Algebraic Reconstruction Technique: Algebraic reconstruction techniques reconstruct an object function f(x,y) by solving a set of linear equations which relate the sampled projections to the desired discrete reconstruction grid [10]. In Figure 2.5 a square grid has been superimposed on an image f(x,y). It is assumed that f(x,y) is constant in each square cell. Also it is assumed that there are total N = n x n cells in the grid and f_m denotes the constant value in the mth cell. In algebraic reconstruction, the ray is defined to have a width τ and the measured projection at a point is called a *raysum*.

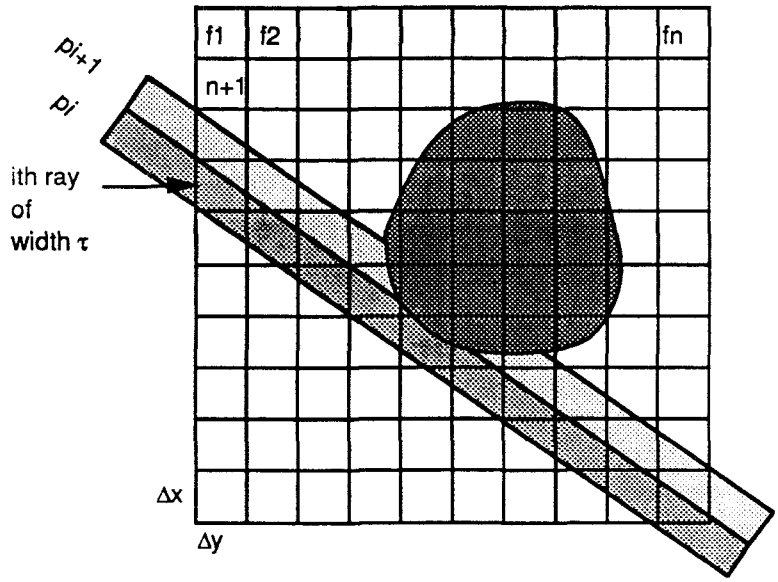

Fig 2.5: For the algebraic reconstruction technique, a rectangular grid is superimposed on the object.

If P_i is the raysum measured with the ith ray, then

$$\sum_{j=1}^{N} w_{ij} f_j = P_i ; \quad i = 1, 2, 3, ..., M \qquad [2.11]$$

where M is the total number of rays in all the projections, and w_{ij} is the weighting factor representing the contribution of the jth cell to the ith raysum. The factor w_{ij} is equal to the fractional area of the jth image cell intercepted by the ith ray. Equation [2.11] can be written in the expanded form as follows:

$$\begin{aligned}
&w_{11} f_1 + w_{12} f_2 + ... + w_{1N} f_N = P_1 \\
&w_{21} f_1 + w_{22} f_2 + ... + w_{2N} f_N = P_2 \\
&..... \quad ..... \quad ..... \qquad [2.12] \\
&..... \quad ..... \quad ..... \\
&w_{M1} f1 + w_{M2} f_2 + ... + w_{MN} f_N = P_M
\end{aligned}$$

For a 256 x 256 size image, N = 65536 and normally M also has the same size. So Equation [2.12] represents approximately a matrix of size 65000 x 65000 and it is solved in an iterative method.

The quality of reconstructed images by this method are not favorable compared to the other two methods and also it needs several iterations to reconstruct the image. Each iteration needs a number of computations comparable to the total number of computations in other methods [9].

Convolution Backprojection Method: The Convolution Backprojection method probably is the most popular algorithm in computer aided tomography. This is simple and tends to give better reconstructions than other approaches. The mathematical model used in this approach was first introduced by Ramachandran and Laksminarayan [7]. This model is also based on the Projection Slice theorem. Shepp and Logan [1] developed a modified model, but the mathematical foundation of both models are essentially the same.

If the Fourier transform $F(\omega_x , \omega_y)$ is known, then the object function f(x,y) is given by

$$f(x,y) = \frac{1}{4\pi^2} \int_{-\infty}^{\infty}\int_{-\infty}^{\infty} F(\omega_x , \omega_y)\, e^{j(\omega_x x+\omega_y y)}\, d\omega_x d\omega_x \qquad [2.13]$$

now if, $\omega_x = \omega \cos\theta$

and $\omega_y = \omega \sin\theta$

then,

$$f(x,y) = \frac{1}{4\pi^2} \int_{0}^{\pi}\int_{-\infty}^{\infty} F(\omega,\theta) e^{j\omega(x\cos\theta + y\sin\theta)}\, |\omega|\, d\omega\, d\theta \qquad [2.14]$$

where $|\omega|$ comes from the Jacobian of the transformation into polar co-ordinates.

By Equation [2.5] $F(\omega , \theta) = P(\omega, \theta)$; and substituting this in Equation [2.14] , we have

$$f(x,y) = \frac{1}{4\pi^2} \int_0^{\pi} \int_{-\infty}^{\infty} P(\omega , \theta)\, e^{j\omega(x\cos\theta + y\sin\theta)}\, |\omega|\, d\omega d\theta \qquad [2.15]$$

At this point, the variable $Q(t,\theta)$ is introduced such that

$$Q(t;\theta) = \frac{1}{2\pi} \int_{-\infty}^{\infty} P(\omega, \theta)\, |\omega|\, e^{j\omega t}\, d\omega \qquad [2.16]$$

where, $t = x\cos\theta + y\sin\theta.$

Equation [2.15] now can be written as

$$f(x,y) = \frac{1}{2\pi} \int_0^{\pi} Q(t,\theta)\, d\theta \qquad [2.17]$$

Equation [2.16] suggests that $Q_\theta(t)$ is the inverse Fourier transform of the product of two Fourier transforms. So $Q_\theta(t)$ can be evaluated by convolving two time domain functions corresponding to I.F.T [$P(\omega,\theta)$] and I.F.T [$|\omega|$], where I.F.T denotes inverse Fourier transform.

I.F.T [$P(\omega,\theta)$] is the measured projection data $p_\theta(t)$ for a particular orientation θ, which is known to us. On the other hand, I.F.T [$|\omega|$] cannot be computed as the function $|\omega|$ does not converge. But in all practical cases, the projection data will be sampled at a regular interval, say a; and under such circumstances, it can be assumed that in the frequency domain the projections do not have any significant energy band outside the frequency interval of (-1/2a, 1/2a).

Based on the previous assumption, the term $|\omega|$ in Equation [2.16] can be replaced by the function $H(\omega)$, where

$$H(\omega) = G(\omega)\, B(\omega)$$

and $G(\omega)$ is some function which approximates $|\omega|$ in the desired frequency range and

$$B(\omega) = 1, \quad \text{when} \quad |\omega| \leq \frac{\pi}{a}$$

$$= 0 \qquad \text{otherwise.}$$

It is now possible to calculate I.F.T $[H(\omega)] = h(t)$ and the following can be written,

$$Q(t;\theta) = \int_{-\infty}^{\infty} p_\theta(\tau)\; h(t-\tau)\; d\tau \qquad [2.18]$$

In the discrete domain, Equation [2.18] can be written as

$$Q(t;\theta) = a \sum_{k=-\infty}^{\infty} p_\theta\,(t_k\,;\,\theta)\; h\;(t - t_k) \qquad [2.19]$$

$$\text{where } t_k = ka; \quad k = 0, \pm 1, \pm 2, \ldots$$

and Equation [2.16] can be written as

$$f(x,y) = \frac{1}{2\pi} \left\{ \frac{\pi}{n} \sum_{j=0}^{j=n-1} a \sum_{k=-\infty}^{\infty} p(t_k, \theta_j) h(t-t_k) \right\}$$

$$= \frac{a}{2n} \sum_{j=0}^{n-1} \sum_{k=-\infty}^{\infty} p(t_k , \theta_j)\ h(x\cos\theta_j + y\sin\theta_j - t_k) \qquad [2.20]$$

where $\theta_i = i\pi/n$; i = 0, 1, ... , n-1.

If it is assumed that $f(x,y) = 0$ for $x^2 + y^2 > 1$, then $p(t;\theta) = 0$ for $|t| > 1$ or $|k| > 1/a$. Hence the sum on k in Equation [2.20] becomes finite.

The choice of the function $G(\omega)$ in Equation [2.17] has been a subject of research [1,7]. The choice is mainly dominated by the requirements of any specific application. Ramachandran and Laksminarayan made a choice corresponding to

$$G(\omega) = |\omega|. \qquad [2.21]$$

which leads to the following impulse response of the filter h(t),

$$h(0) = \frac{\pi}{2a^2}$$

$$h(na) = 0 , \qquad \text{for n = even}$$

$$h(na) = -\frac{2}{\pi n^2 a^2} \qquad \text{for n= odd} \qquad [2.22]$$

Another important choice for the function $G(\omega)$, made by Shepp and Logan, is

$$H(\omega) = \left| \frac{2}{a} \sin\frac{\omega a}{2} \right| \qquad [2.23]$$

leading to the impulse response

$$h(0) = \frac{4}{\pi a^2}$$
$$h(na) = -\frac{4}{\pi a^2(4n^2 - 1)} \qquad [2.24]$$

Shepp and Logan's filter is less sensitive to noise at the expense of reduced resolution corresponding to high frequency components. This thesis specifically deals with the function $G(\omega) = |\omega|$.

Aliasing and Artifacts in Reconstructed Images: In all practical applications, projections are measured at some sample points and that is the only knowledge available about the data. According to the sampling theorem if the Fourier transform of a function is to be calculated from its samples, it must be sampled at a rate twice the highest frequency content of the signal. In all practical cases the object and hence the projection is of finite duration. This suggests that the Fourier transform of the projections will be of infinite duration in the frequency domain. If the measured projections have smooth edges, then the higher frequency components of the signals will have less energy. When such a signal is sampled and its Fourier

transform is computed, there will always be some aliasing error present in the result.

When implementing the direct Fourier reconstruction technique, the discrete Fourier transform of the projections is calculated as suggested by Equation [2.7]

$$F(k;\theta) = \sum_{n=-N/2}^{N/2} p(n\ ;\ \theta)\ e^{-j\frac{2\pi}{N+1}nk}$$

In light of the previous discussion, $F(k\ ;\ \theta)$ is corrupted by the aliasing effect.

Theoretically an infinite number of projections are required for reconstructing a function; but in practice, only a finite number of projections are measured. This also causes artifacts in the reconstructed image.

In the Convolution Backprojection method, each projection is convolved with a so called $|\omega|$ filter. In using that filter it is assumed that the projections do not have any frequency content outside the range (-1/2a, 1/2a). As has been discussed, a projection with finite duration will have energy at all frequencies and the calculated $Q(t,\theta)$ in Equation [2.19] will have contaminations.

In the end, although errors exist, they can be reduced very much by using the reconstruction techniques under practical conditions which closely follow the assumptions made. For example, these algorithms will work better for objects with smooth projections, because under such conditions the higher frequency content of the signals can be practically neglected.

CHAPTER III

TRUNCATED $|\omega|$ FILTER FOR IMAGE RECONSTRUCTION

Introduction: One of the steps involved in the Convolution Backprojection method is to generate modified projections by convolving projection data with a filter which approximates the $|\omega|$ filter within the frequency range of interest. Although it is possible to reconstruct good quality images with a finite length impulse response filter, it is seen that the quality of the image depends upon the length of the filter.

Filters having finite length impulse response are characterized by localized errors. That may cause significant distortions in reconstructed images. In this chapter, such errors are characterized and the processes which may reduce such errors are discussed so that better quality images can be reconstructed by short length filters. Although the mathematical model used for image reconstructions by the Convolution Backprojection method has been introduced in the last chapter, the discussion in this chapter starts with the model equation and then leads to the characterization of the errors in approximate $|\omega|$ filters.

Reconstruction Model : It has been shown in Equation [2.15] that if $P(\omega,\theta)$ represents the Fourier transform of the projection measured at the θ angle orientation, then the object value at any co-ordinate (x,y) can be expressed as

$$f(x,y) = \frac{1}{4\pi^2} \int_0^{\pi} \int_{-\infty}^{\infty} P(\omega,\theta)\, e^{j\omega(x\cos\theta+y\sin\theta)}\, |\omega|\, d\omega d\theta$$

$$= \frac{1}{2\pi} \int_0^{\pi} \left\{ \frac{1}{2\pi} \int_{-\infty}^{\infty} P(\omega,\theta)\, |\omega|\, e^{j\omega(x\cos\theta+y\sin\theta)}\, d\omega \right\} d\theta$$

The integral within the curly bracket represents the inverse Fourier transform of the product of the two individual Fourier transforms $F_1(\omega) = P(\omega;\theta)$ and $F_2(\omega) = |\omega|$. The properties of the Fourier transform suggests that this integral can be calculated by convolving two time domain functions corresponding to $F_1(\omega)$ and $F_2(\omega)$, provided that the inverse Fourier transform of both functions exists. The time domain function corresponding to $F_1(\omega)$ is $p(t;\theta)$, which is the measured projection for a particular orientation; but the function $\int_{-\infty}^{\infty} |\omega|\, d\omega$ is not finite, leading to the conclusion that the inverse Fourier transformation of $|\omega|$ does not exist.

Now, for most practical cases the measured projection will be smooth and hence will have frequency spectrums with significant energy content only in some low frequency band. The higher frequency content will be gradually insignificant and after a certain frequency range they can be neglected without introducing much of an error. Some logical choice has to be made at this point for the cut off frequency.

For processing data in a digital computer, all the data have to be digitized including the measured projections. If the sampling interval

is denoted by 'a', then the Nyquist frequency is 1/2a and it can be assumed that there is no energy in the measured signal beyond the frequency interval (-1/2a,1/2a). Accordingly one may replace the $|\omega|$ function with another which approximates this function only within the angular frequencies $(-\pi/a,\pi/a)$. One choice may be denoted by $H(\omega) = |\omega| B(\omega)$, where,

$$B(\omega) = 1, \text{ for } |\omega| \leq \frac{\pi}{a}$$

$$= 0, \quad \text{otherwise.}$$

Such a function is shown in Figure 3.1. This function is suggested by Ramachandran and Laksminarayan [7].

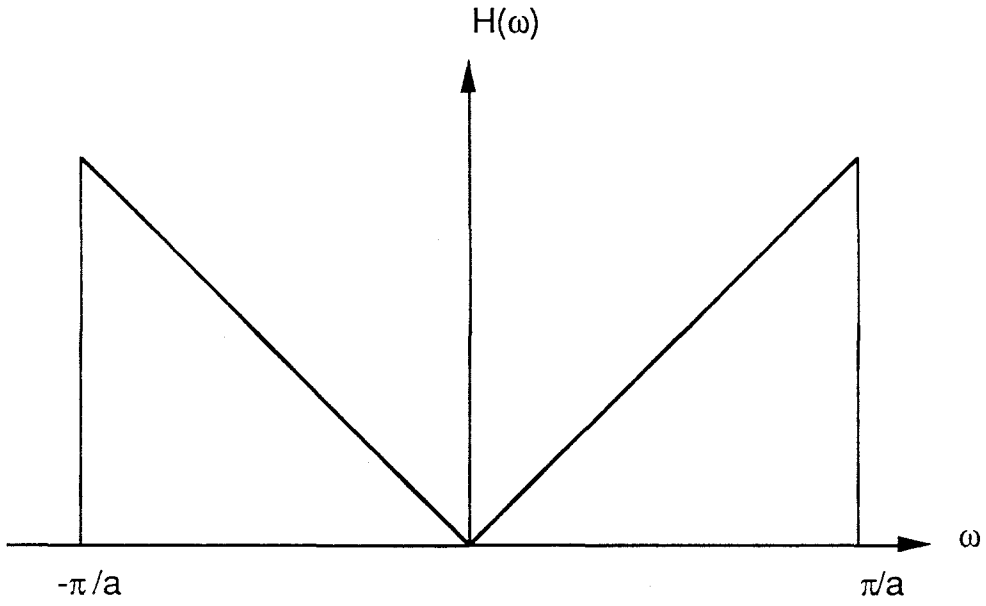

Fig 3.1: The transfer function of the $|\omega|$ filter which is band limited to an angular frequency π/a.

It is evident that the integral $\int_{-\infty}^{\infty} |H(\omega)|\, d\omega$ is finite and so its Fourier transform exists. The impulse response h(t) of the filter H(ω) can be shown to be

for $t = 0$,

$$h(0) = \frac{\pi}{2a^2}$$

for $t \neq 0$,

$$h(t) = \frac{1}{\pi} \left[-\frac{1}{t^2} + \frac{1}{t^2} \cos\frac{\pi}{a} t + \frac{\pi}{ta} \sin\frac{\pi}{a} t \right] \qquad [3.1]$$

If h(t) is sampled at the same rate as the measured projection, t can be replaced by na in Equation [3.1], where $n = \pm 1, \pm 2, \ldots\ldots \ldots$, which gives

$$h(na) = \frac{1}{\pi} \left[-\frac{1}{n^2a^2} + \frac{1}{n^2a^2} \cos\frac{\pi}{a} na + \frac{\pi}{na^2} \sin\frac{\pi}{a} na \right] \qquad [3.2]$$

replacing h(na) by h(n), Equation [3.2] can be written as

$$h(n) = \frac{1}{\pi} \left[-\frac{1}{n^2a^2} + \frac{1}{n^2a^2} \cos n\pi \right]$$

so when n is odd,

$$h(n) = -\frac{2}{\pi\, n^2a^2}$$

and when n is even,

$$h(n) = 0. \qquad [3.3]$$

The sampled impulse response is shown in Figure 3.2.

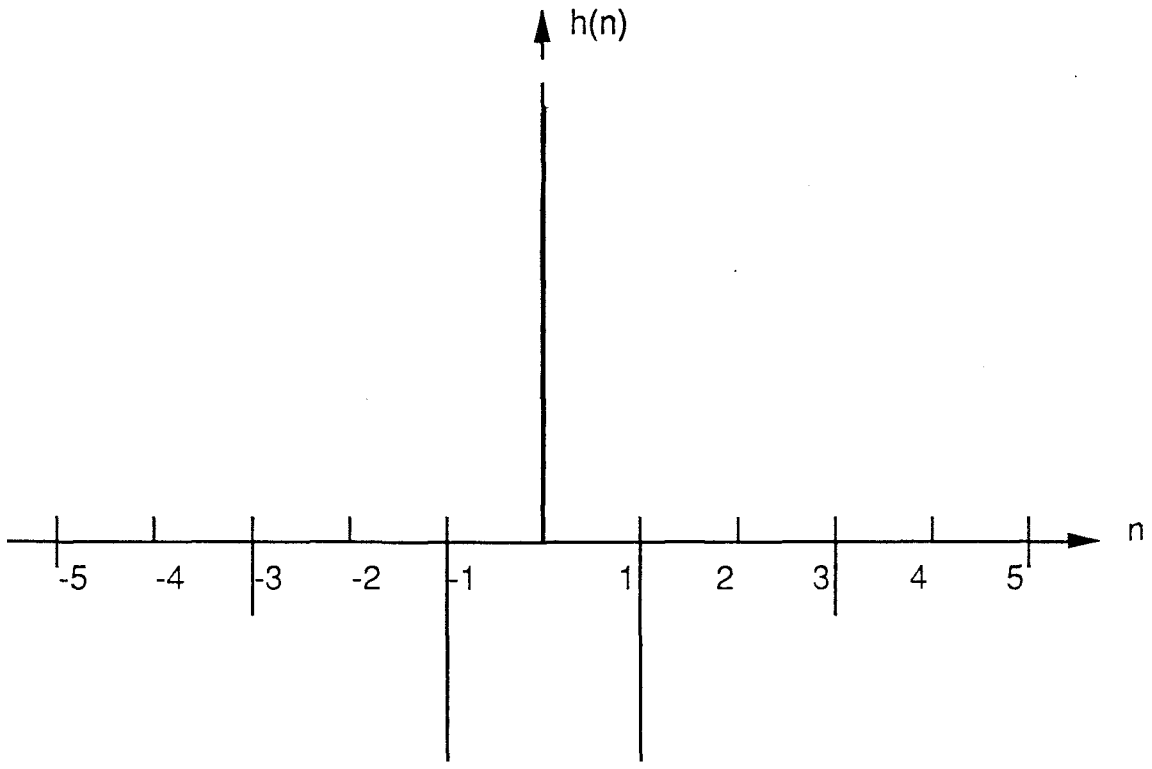

Fig 3.2: The unit sample response of the transfer function shown in Figure 3.1.

Note that h(n) extends to infinity in both directions. But if there are K samples in the measured projection, it is sufficient to calculate K samples of the modified projections by convolving the measured projection data with the filter. This result may be computed by direct convolution and 2K-1 samples of the filter are required for exact evaluation. The expression is given by

$$Q(n;\theta) = a \sum_{m=-K}^{K} p(m;\theta)\, h(n-m) \qquad [3.4]$$

The results of modified projections between two samples are generated by interpolation. In this thesis linear interpolation has been used as suggested by Shepp and Logan [1].

The important point is that, while generating samples of modified projections, the measured projection data can see only 2K-1 samples of the impulse response of the $H(\omega)$ filter. The frequency response of these 2K-1 samples are not exactly the same as that of $H(\omega)$ filter.

Error in Finite Length $|\omega|$ Filter : K samples of the modified projection can be calculated from K samples of the measured projections and 2K-1 samples of the impulse response of the $|\omega|$ filter. Also, since the frequency response of the $|\omega|$ filter is band limited, its impulse response is of infinite duration. It is obvious that 2K-1 samples of the $|\omega|$ filter do not offer the ideal frequency response and hence there are always some errors between the frequency responses of the 2K-1 samples of the impulse response and the desired one. These errors are characterized in this section.

Choosing 2K-1 samples from an infinite duration impulse response is the same as multiplying the ideal impulse response with a rectangular window of unit hight and appropriate width. That is, if

the samples of the infinite duration impulse response are expressed as $h_d(n)$ and the samples of the truncated filter are denoted by h(n), then

$$h(n) = h_d(n)\, w(n) \qquad [3.5]$$

where,

$$w(n) = 1 , \quad -(K-1) \le n \le K-1$$
$$= 0 , \quad \text{otherwise.}$$

If the Fourier transform is applied in both sides of Equation [3.5] , it can be written as

$$H(\omega) = \frac{1}{2\pi} \int_{-\pi}^{\pi} H_d(\Omega)\, W(\omega-\Omega)\, d\Omega \qquad [3.6]$$

That is, $H(\omega)$ is the continuous convolution of the desired frequency response with the Fourier transform of the window. Thus the actual frequency response will be the smeared version of the desired response $H_d(\omega)$.

It is often the intention of a designer to achieve the 'best' frequency response of a filter for a given length N. Of course, the definition of the word 'best' is dependent on the error criterion defined for the design. Finite duration filters designed by applying a rectangular window in the time domain have minimum squared integral error in the frequency response. This is a well known result and is shown below.

Integral squared error is defined as the integral of the squared difference between the actual and the desired frequency response over the basic frequency range $-\pi \leq \omega \leq \pi$. If this error is denoted by E, then

$$E = \frac{1}{2\pi} \int_{-\pi}^{\pi} |H(\omega) - H_d(\omega)|^2 \, d\omega \qquad [3.7]$$

$H(\omega)$ is the real function for the $|\omega|$ filter under discussion. Assuming that the length of the truncated filter is 2N-1 and is symmetric about the origin, the following relationships can be written,

$$H(\omega) = \sum_{n=-N}^{N} h(n) \, e^{-j\omega n}$$

$$h(n) = \frac{1}{2\pi} \int_{-\pi}^{\pi} H(\omega) \, e^{j\omega n} \, d\omega$$

$$H_d(\omega) = \sum_{n=-\infty}^{\infty} h_d(n) \, e^{-j\omega n}$$

and $$h_d(n) = \frac{1}{2\pi} \int_{-\pi}^{\pi} H_d(\omega) \, e^{j\omega n} \, d\omega$$

According to Parseval's theorem, the energy in a signal can be calculated in the time domain as well as in the frequency domain. That is, if the samples of a signal are denoted by x(n) and its Fourier transform as $X(\omega)$ then

$$\sum_{n=-\infty}^{\infty} |x(n)|^2 = \frac{1}{2\pi} \int_{-\pi}^{\pi} |X(\omega)|^2 \, d\omega \qquad [3.8]$$

Applying this principle to Equation [3.7], it can be written that

$$E = \frac{1}{2\pi} \int_{-\pi}^{\pi} |H(\omega) - H_d(\omega)|^2 \, d\omega$$

$$= \sum_{n=-\infty}^{\infty} |h(n) - h_d(n)|^2 \qquad [3.9]$$

Since h(n) is of finite duration, from -(N-1) to (N-1) only, Equation [3.9] can be written as

$$E = \sum_{n=-N+1}^{N-1} |h(n) - h_d(n)|^2 + 2 \sum_{n=N}^{\infty} |h_d(n)|^2 \qquad [3.10]$$

It is obvious in Equation [3.10] that E is minimum if h(n) is identical to $h_d(n)$ for the values of n from -N+1 to N-1.

The above analysis shows that if a finite number of the samples of the impulse response of the $|\omega|$ filter are used to compute modified projections, then the frequency response of the filter has minimum integral square error when compared to the desired frequency response.

Although the error in a truncated $|\omega|$ filter using rectangular window is optimum in the least square sense, the error is localized heavily where the function has a discontinuity in its derivative. This is the well known "Gibbs phenomenon". The desired frequency response has a discontinuity in its derivative at $\omega=0$ and two other at $\omega = \pm \pi$. The error in the neighborhood of $\omega = \pm \pi$ is not of intense attention. because in most practical cases the measured projections have spectrums with large amplitudes near the origin. The amplitude of the spectrums in those cases decrease with an increase in frequency letting the $|\omega|$ filter tolerate larger errors near $\omega = \pm\pi$ for good quality image reconstructions.

The Fourier transform $W(\omega)$ of $w(n)$ defined in Equation [3.5] is given by

$$W(\omega) = \sum_{n=-K+1}^{K-1} e^{-j\omega n} = \sum_{k=0}^{2K-2} e^{-j\omega k}\, e^{j\omega(K-1)}$$

$$= \frac{1 - e^{-j\omega(2K-1)}}{1 - e^{-j\omega}}\; e^{j\omega(K-1)}$$

$$= \frac{e^{j\omega(2K-1)/2} - e^{-j\omega(2K-1)/2}}{e^{j\omega/2} - e^{-j\omega/2}}$$

$$= \frac{\mathrm{Sin}\left\{\frac{\omega}{2}(2K-1)\right\}}{\mathrm{Sin}\frac{\omega}{2}} \qquad [3.11]$$

Equation [3.6] suggests that having W(ω) as narrow as possible causes H(ω) to approximate $H_d(\omega)$ closely. The width of the main lobe of W(ω) decreases as K increases. The maximum length of the filter for calculating the modified projections can be N=2K-1 and it is of interest here to investigate the approximation error as N is decreased.

The oscillating nature of W(ω) causes the integral W(ω−Ω) H(Ω) in Equation [3.6] to vary in a oscillatory manner and Figure 3.3 shows the error in the truncated |ω| filter as a function of frequency for N= 63. From the figure it is evident that the maximum error in the low frequency range occurs at ω=0. This error E(0) is given simply by the algebraic summation of the samples of the impulse response. E(0) has a positive value at zero frequency for finite filter length. The magnitude of E(0) increases as N is decreased. This can be observed in Figure 3.4. Figure 3.4 shows the error in the |ω| filter for N=31.

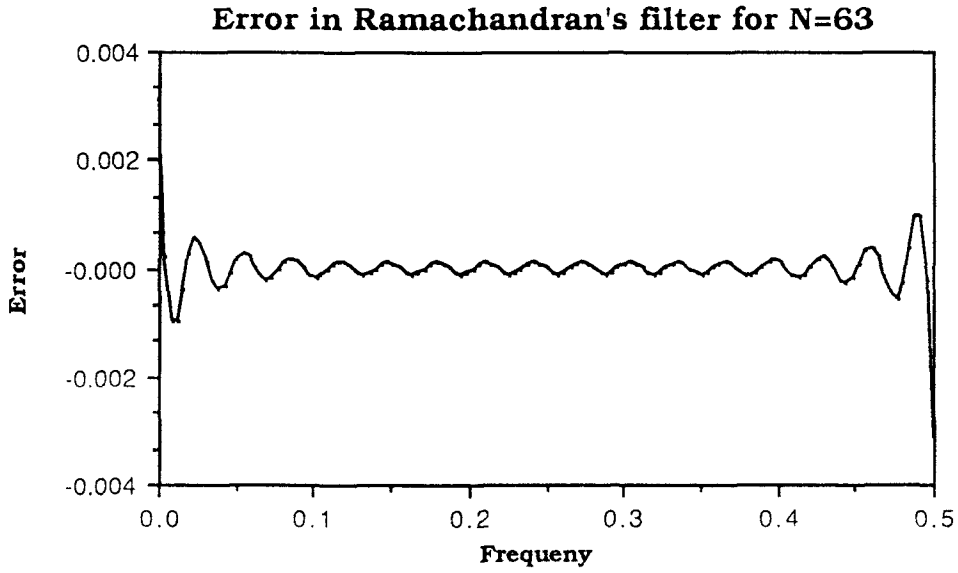

Fig 3.3: Error in Ramachandran's |ω| filter for N=63.

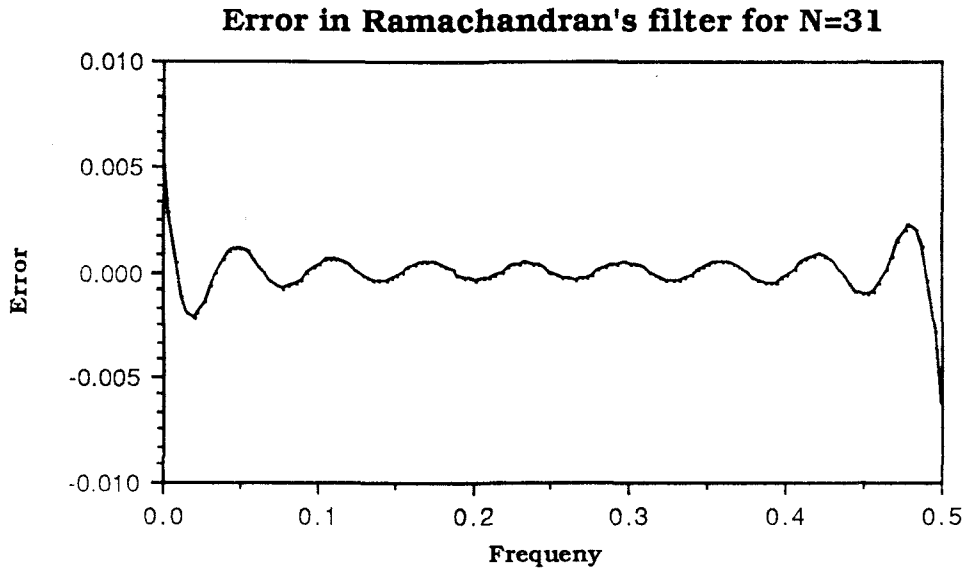

Fig 3.4: Error in Ramachandran's $|\omega|$ filter for N=31.

A direct comparison between the errors in Ramachandran's filters for N=63 and N=31 is given in Figure 3.5 where the previous two graphs have been drawn in the same frame. The zero frequency

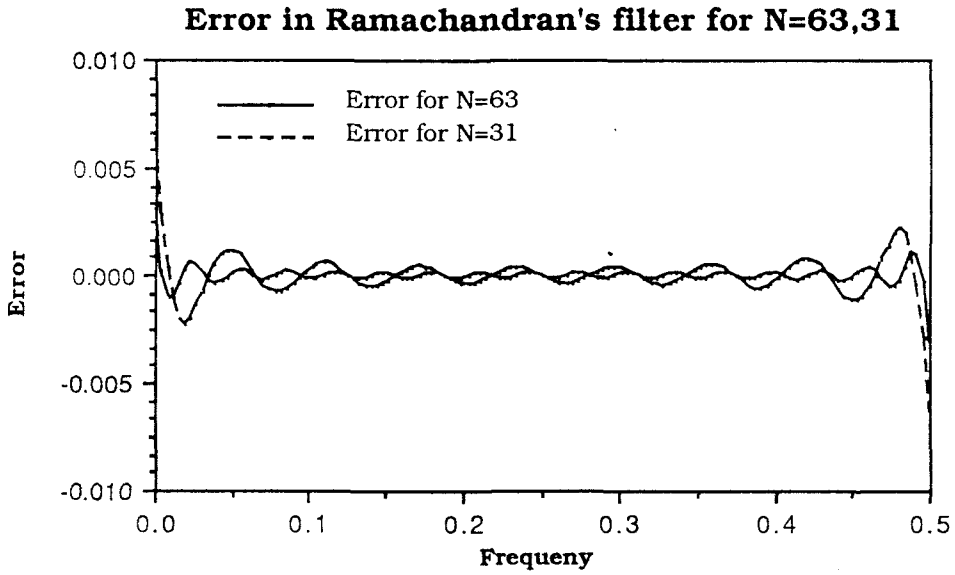

Fig 3.5: Comparison of the error in Ramachandran's filter for for N=63 and N=31.

error for the above two filters with N=63 and N=31 are .00317 and .00632 respectively.

Weighted Least Square Error Filter: The frequency response $H(\omega)$ of a finite length impulse response filter is given by

$$H(\omega) = \sum_{n=-N+1}^{N-1} h(n)\, e^{-j\omega n} \qquad [3.14]$$

The frequency response of the $|\omega|$ filter is a real function and also even about the origin $\omega=0$. By the property of the Fourier transform, $h(n)$ will also be a real function and even about $n=0$; that is, $h(n) = h(-n)$. In this case, Equation [3.14] can be written as

$$H(\omega) = h(0) + h(1)\{e^{j\omega n} + e^{-j\omega n}\} + h(2)\{e^{j2\omega n} + e^{-j2\omega n}\} + \ldots$$

$$= h(0) + 2\sum_{n=1}^{N-1} h(n)\cos\omega n \qquad [3.15]$$

If the values of $h(n)$ of the approximate filter are equal to the values of $h_d(n)$ of the desired filter, it has been mentioned in the previous section that the filters represented by Equation [3.15] correspond to a frequency response with minimum integral square of the approximation error. Although this error is minimum in the least square sense, it has been shown that it is concentrated heavily in some specific areas of the frequency range. As a result, reconstructed

images contain heavy distortions corresponding to those frequencies. Reconstruction from truncated filters are improved by reducing the error from the frequency ranges where the signals have significant level of amplitudes, low frequencies in this case. This can lead to reconstruction of images with significantly short filters. One technique of designing such filters is the weighted least square approach suggested by Lewitt [6].

The formulation of the design problem may start from sampling the frequency range of interest at M equally spaced points. If the sampling starts at ω=0, then the frequency samples are located at

$$\omega_k = \frac{2\pi k}{M}, \qquad k= 0, 1, 2, \ldots\ldots, M-1.$$

On the other hand, if there is no sample at ω=0, then the samples are located at

$$\omega_k = \frac{(2k+1)\pi}{M}, \qquad k= 0, 1, 2, \ldots\ldots, M-1.$$

The samples of the desired frequency response can be denoted by $H_d(\omega_k)$ and the samples of the actual frequency response can be represented by $H(\omega_k)$. $H(\omega_k)$ can be written from Equation [3.15] as follows,

$$H(\omega_k) = h(0) + \sum_{n=1}^{N-1} 2h(n) \operatorname{Cos} \omega_k n \qquad [3.16]$$

Substituting $x_{kn} = 2 \text{ Cos } \omega_k n$, $H(\omega_k) = H(k)$ and $H_d(\omega_k) = H_d(k)$, Equation [3.16] stands as

$$H(k) = h(0) + h(1)\, x_{k1} + h(2)\, x_{k2} + \ldots\ldots + h(N-1)\, x_{k(N-1)}$$

If the error between the desired and the actual frequency response is expressed as e(k), the following can be written.

$$H(k) = H_d(k) + e(k)$$

$$\text{or} \qquad e(k) = H_d(k) - H(k) \qquad [3.17]$$

The square error can be written as

$$e^2(k) = [\, H_d(k) - H(k)]^2$$

and the weighted square error can be expressed as

$$e_w^2(k) = W(k)\, [H_d(k) - H(k)]^2$$

The total of the weighted square errors over all the sample points is given by

$$E = \sum_{k=0}^{M-1} e_w^2(k)$$

$$= \sum_{k=0}^{M-1} W(k)[H_d(k) - \{h(0) + h(1)\, x_{k1} + h(2)\, x_{k2} + \ldots\ldots + h(N-1)\, x_{k(N-1)}\}]^2$$

The objective is to choose h(0), h(1), ... , h(N-1) such that the total square error E is minimized. Under such conditions, the following relationships must hold.

$$\frac{dE}{dh(n)} = 0, \quad \text{for } n = 0, 1, \ldots\ldots, N-1. \qquad [3.18]$$

Equation [3.18] gives the following set of equations.

$$2\sum_{k=0}^{M-1} W(k)[H_d(k) - \{h(0) + h(1)\, x_{k1} + \ldots\ldots + h(N-1)\, x_{k(N-1)}\}] = 0$$

$$2\sum_{k=0}^{M-1} W(k)[H_d(k) - \{h(0) + h(1)\, x_{k1} + \ldots\ldots + h(N-1)\, x_{k(N-1)}\}]\, x_{k1} = 0$$

....

....

$$2\sum_{k=0}^{M-1} W(k)[H_d(k) - \{h(0) + h(1)\, x_{k1} + \ldots\ldots + h(N-1)\, x_{k(N-1)}\}]\, x_{k(N-1)} = 0$$

The above set of equations holds for the expression

$$\mathbf{X^T W X h = X^T W H_d} \qquad [3.19]$$

where,

$$\mathbf{X} = \begin{bmatrix} 1 & x_{11} & x_{12} & \cdots & x_{1(N-1)} \\ 1 & x_{21} & x_{22} & \cdots & x_{2(N-1)} \\ \cdots & \cdots & \cdots & \cdots & \cdots \\ \cdots & \cdots & \cdots & \cdots & \cdots \\ 1 & x_{(M-1)1} & x_{(M-1)2} & \cdots & x_{(M-1)(N-1)} \end{bmatrix}$$

$$\mathbf{W} = \begin{bmatrix} W(0) & 0 & 0 & \cdots & 0 \\ 0 & W(1) & 0 & \cdots & 0 \\ 0 & 0 & W(2) & \cdots & 0 \\ \cdots & \cdots & \cdots & \cdots & \cdots \\ \cdots & \cdots & \cdots & \cdots & \cdots \\ 0 & 0 & 0 & \cdots & W(M-1) \end{bmatrix}$$

$$\mathbf{h} = \begin{bmatrix} h(0) \\ h(1) \\ \cdots \\ \cdots \\ h(N-1) \end{bmatrix} \quad \text{and} \quad \mathbf{H_d} = \begin{bmatrix} H_d(0) \\ H_d(1) \\ \cdots \\ \cdots \\ H_d(M-1) \end{bmatrix}$$

Equation [3.19] can be solved for h(n), where n = 0, 1, 2, ..., N-1, by numerical analysis techniques for solving simultaneous equations.

The quality of the reconstructed image depends upon the choice of the weighting function. It has been discussed earlier that for the least square error filter, which has uniform error weighting, the

error is large near zero frequency, then minimum for intermediate frequencies and again large near the Nyquist frequency. For most practical images, the measured projections have spectrums with large amplitudes at low frequencies and decreasing amplitudes as the frequency increases. This suggests that errors in the frequency response near zero frequency have significant impact on the quality of reconstructed images. On the other hand, since the spectral amplitude of the signals are very low at the high frequencies, the error tolerance at higher frequencies may be higher than that for lower frequencies. This kind of discussion leads to the choice of a weighting function which has large values at low frequencies and decreases as the frequency increases. Lewitt et. al have suggested $1/\omega^2$ as an appropriate weighting function. Figure 3.6 shows the error in the frequency response of the $|\omega|$ filter for this weighting

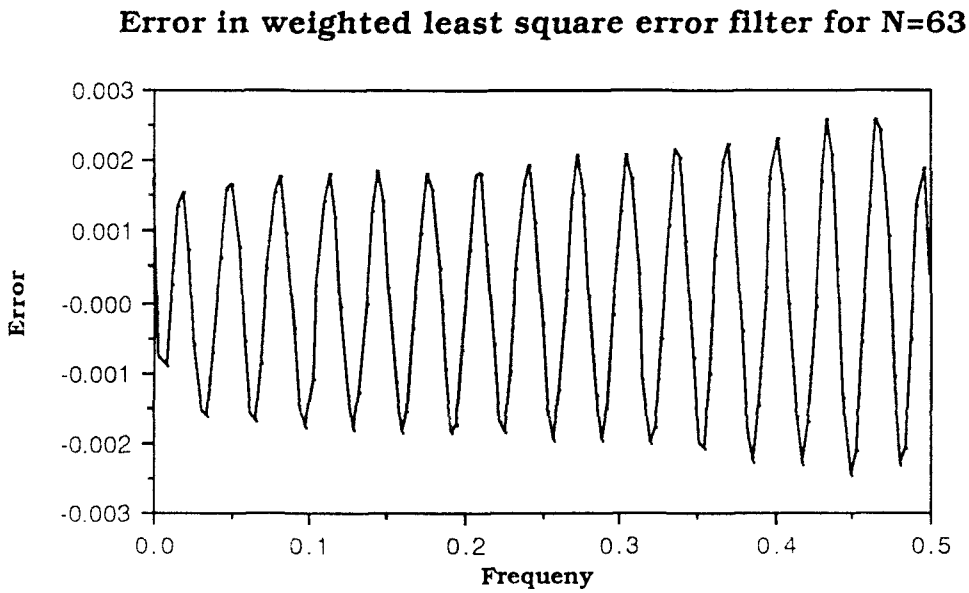

Fig 3.6: Error in weighted least square error filter for N=63.

function. For N=63, the zero frequency error for this filter is .00172. This error is less than Ramachandran's filter with N=63 but it is clearly seen here that the error increases with increasing frequency.

CHAPTER IV

SIMULATION RESULTS AND DISCUSSION

Introduction: Various models for image reconstruction from projections have been introduced in Chapter II and the Convolution Backprojection method has been discussed in more detail in chapter III. The later chapter also included discussion about approximating the $|\omega|$ filter with fewer samples of the unit sample response. Various types of errors present in different approximations have also been discussed in that chapter. The present chapter deals with the application of different approximations for image reconstruction. Simulation results have been introduced here along with an analysis of the errors in the reconstructed images. The discussion starts with the process of generating the projection data for the simulations.

Generation of Data for Simulation: Simulation results presented in this chapter are for the image shown in Figure 4.1. This image has similarities with the so called "head phantom" introduced by Shepp and Logan [1]. Such images have been used in research work to test the accuracy of an algorithm to reconstruct cross sections of human head with X-ray tomography. Accuracies of the short filters have also been tested for the same kind of image. Reconstruction of the human head is believed to demand very high numerical accuracy and freedom of artifacts from a reconstruction method.

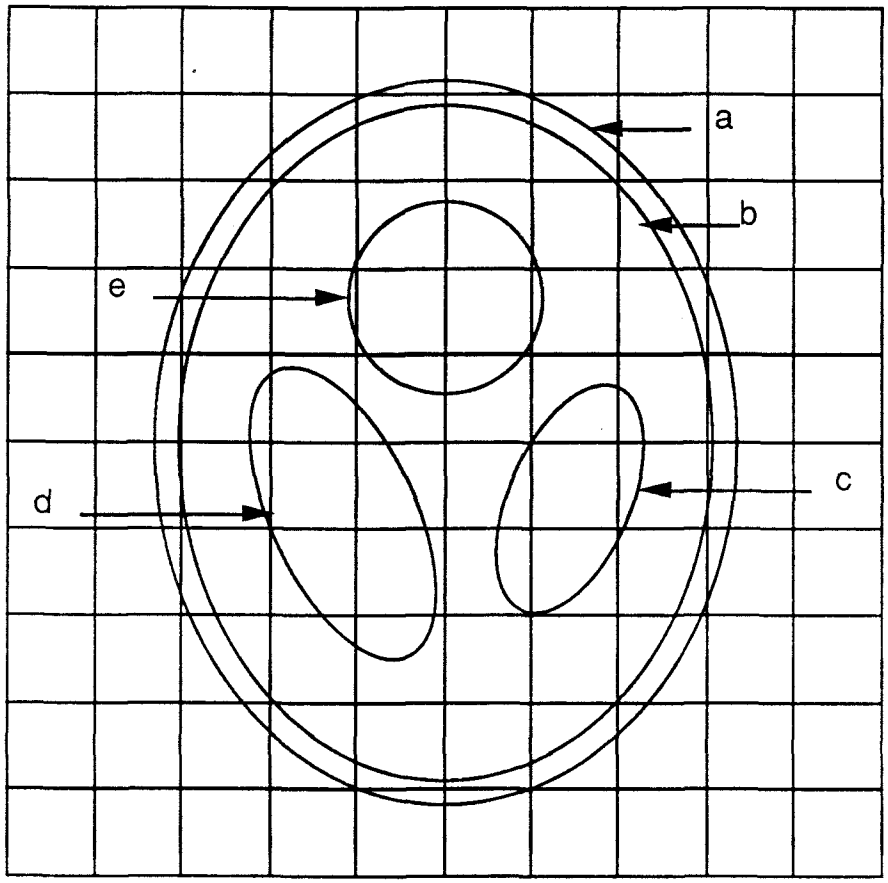

Figure 4.1: Simulated image of a brain phantom.

Table 4.1

Specifications of the ellipses in Figure 4.1

ellipse	center	major axis	minor axis	rotation angle in degree	grey level
a	0,0	.75	.906	0	200
b	0,0	.703	.859	0	-80
c	.328, -.125	.203	.344	22.5	-55
d	-.328, -.125	.203	.5	-22.5	-55
e	0, .344	.25	.25	0	40

Figure 4.1 consists of five ellipses. Specifications are given in Table 4.1. The advantage of using such an image for computer simulation is that one can write analytic expressions for the projection of the image.

The projection of an image composed of multiple ellipses is simply the sum of the projections of the individual ellipses. Rosenfield and Kak [10] have given an expression for the projection of f(x,y) shown in Figure 4.2 as

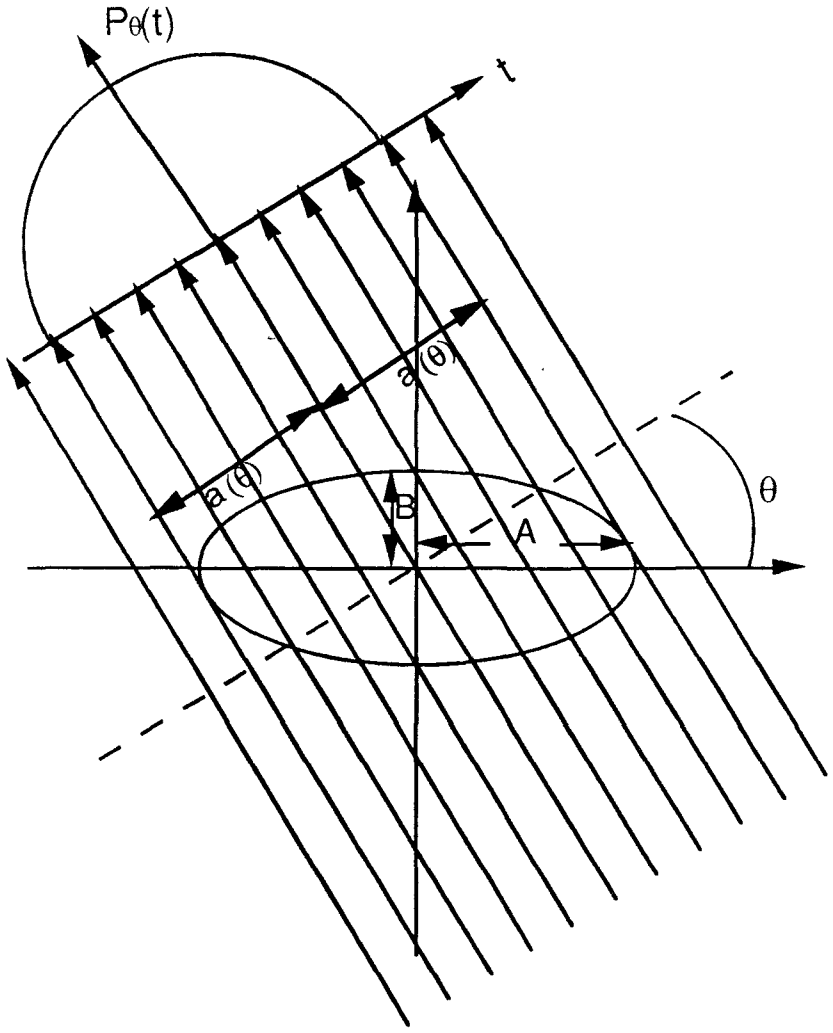

Figure 4.2: Illustration of a projection of an ellipse. The grey level in the interior of the image is ρ and zero outside.

$$P_\theta(t) = \frac{2\rho AB}{a^2(\theta)} \sqrt{a^2(\theta) - t^2} \qquad \text{for} \quad |t| \le a(\theta)$$

$$= 0 \qquad \text{for} \quad |t| > a(\theta)$$

where $a^2(\theta) = A^2 \, Cos^2\theta + B^2 \, Sin^2\theta$

and $f(x,y) = \rho \qquad \text{for} \; \frac{x^2}{A^2} + \frac{y^2}{B^2} \le 1$

$$= 0 \qquad \text{otherwise.}$$

For any ellipse centered at (x_1,y_1) and rotated by an angle β, the projection $P'_\theta(t)$ has also been shown to be

$$P'_\theta(t) = P_{\theta - \beta} \; (t - s \, Cos(\gamma - \theta))$$

where $s = \sqrt{x_1^2 + y_1^2}$ and $\gamma = \tan^{-1} \left(\frac{y_1}{x_1} \right)$.

Using the above expressions, the projections for the image in Figure 4.1 have been calculated for one hundred equally spaced orientations within $0 \le \theta \le \pi$.

Simulation Results: In this section the results of different reconstruction attempts have been presented for different filter lengths N of the $|\omega|$ filters designed by different approaches. In all the cases the image sizes are 128 x 128 pixels and each projection has also been sampled at 128 equally spaced points. Also in each case, one hundred projections from one hundred equally spaced angles have

been considered. Linear interpolation has been used to calculate the values of the modified projections in intermediate points.

Least Square Error Filter: Figure 4.3a shows the reconstructed head phantom for Ramachandran's filter of length N = 255. The unit sample response of this filter has been obtained by sampling the inverse Fourier transform of the desired frequency response, and so it represents a least square error filter. Figure 4.3b shows a numerical comparison between the grey levels of the actual and the reconstructed images along the line y = .017, which is the sixty fourth row of the image. This is the best reconstruction possible for this filter for the given number of samples per projection. This is because, if there are K samples in the measured projection, K samples of the modified projection can be generated by maximum 2K - 1 samples of the unit sample response of the $|\omega|$ filter. From now on, all numerical comparisons between the grey levels of the reconstructed image and the actual image along a particular line will refer to the line y = .017.

Figure 4.4 shows the reconstruction of the same image by the same kind of filter of length N = 127. Comparison of the numerical values in Figure 4.4b shows that this reconstruction is of comparable accuracy with that in Figure 4.3. This is due to the fact that magnitudes h(n) of the unit sample response given by equation [3.3] becomes very small as n increases to large values. Those small values of h(n) do not contribute significantly in the result of the convolution when the modified projections are generated. This type of truncation

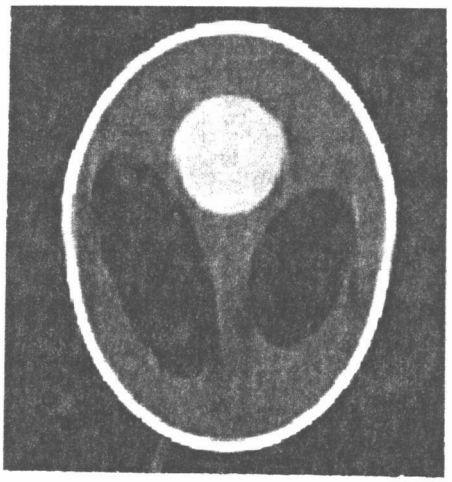

4.3a Reconstructed image bv Ramachandran's filter for N=255

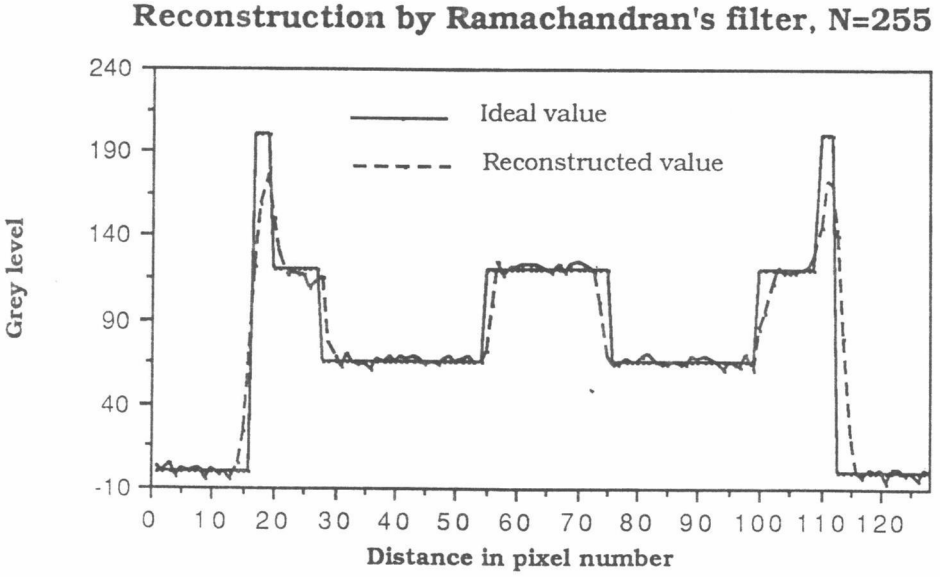

Fig 4.3b: Comparison of the reconstruction of the head phantom along y=.017 line using Ramachandran's filter of length 255.

of the unit sample response of the $|\omega|$ filter by rectangular window has been proposed by Edelheit et. al. [5] for image reconstruction from diverging X-rays. But this approach reaches a limiting point vary fast as the length of the filter is decreased as shown in Figure 4.5.

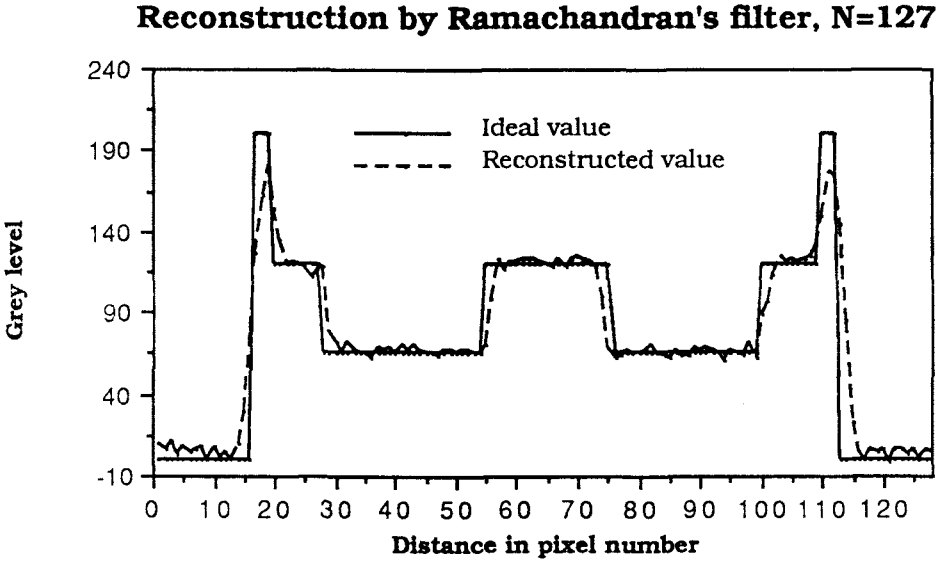

Fig 4.4: Comparison of the reconstruction of the head phantom along y=.017 line using Ramachandran's filter of length 127.

Figure 4.5 shows the result of reconstruction of the same object for length N = 47. The difference between the reconstructed and the desired image values are obvious in Figure 4.5. It was shown in chapter III that as the length of the unit sample response of the $|\omega|$ filter is shortened, the error at zero frequency goes up. This is true for other low frequencies also. These errors become significant when the length of the filter is N = 47 for projections of the image under consideration. Each of the modified projections in this case is

contaminated by zero and low frequency error and so the final reconstruction has a upward shift with other low frequency errors.

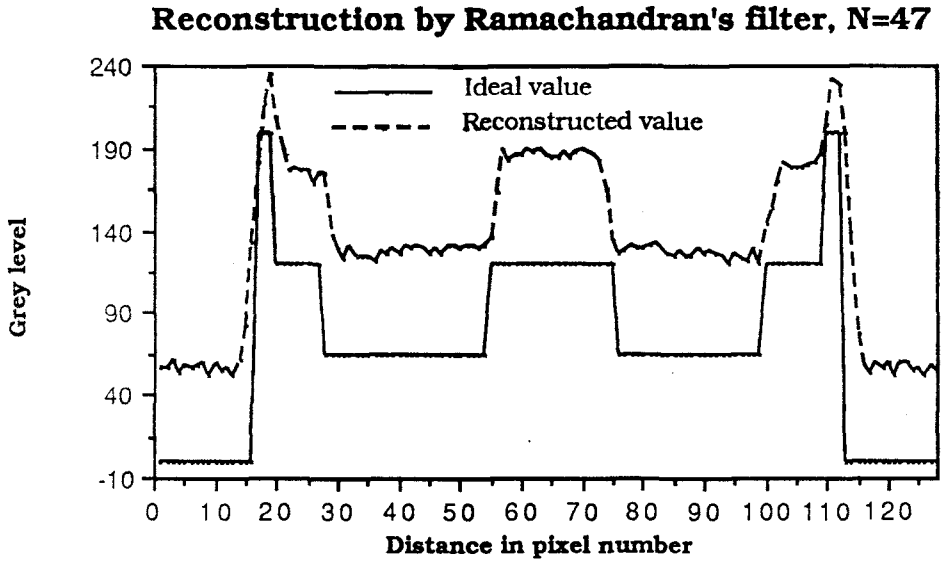

Fig 4.5: Comparison of the reconstruction of the head phantom along y=.017 line using Ramachandran's filter of length 47.

Weighted Least Square Error $|\omega|$ Filter: In the case of least mean square error filters, it has been shown that as the length of the filter is decreased, the low and high frequency approximation error increases. But, since most projections measured in practical applications have very small Fourier coefficients near the Nyquist frequency, the approximation error for the $|\omega|$ filter at higher frequencies may have larger magnitudes. On the other hand, the Fourier coefficients of the measured projections are large at low frequencies and the approximation may have very little tolerance for errors at those frequencies. Figure 4.6 shows the result of the

reconstruction of the head phantom for a weighted least square filter of length N=255. The weighting function used is $1/\omega^2$.

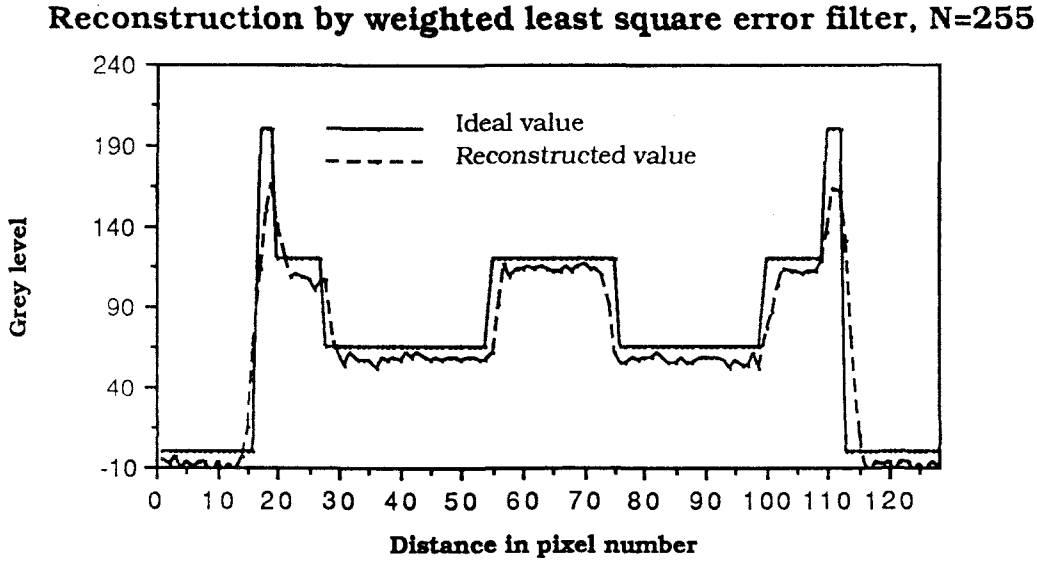

Fig 4.6: Comparison of the reconstruction of the head phantom along y=.017 line using weighted least square error filter of length 255.

Figure 4.7 shows the reconstruction of the head phantom for the filter of length N=47. Comparing the numerical values between the desired image and this reconstructed image along the line y = .017, it is obvious that this filter gives better reconstruction than the filter used in Figure 4.5. This is because of the nature of the weighting function $1/\omega^2$. This function has been suggested by Lewitt et. al. [6] and weights errors at low frequencies heavily. In the mid-frequency range, the least mean square error filter contains a very small approximation error and a lower weighting offered by $1/\omega^2$ works

satisfactorily. At higher frequencies, very small values of the weighting function causes the approximation errors in the designed

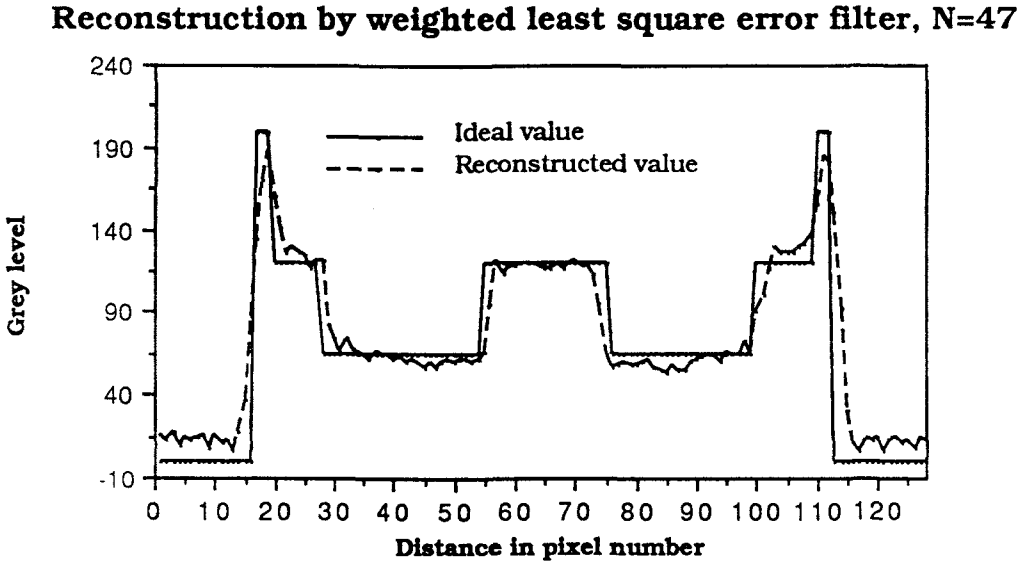

Fig 4.7: Comparison of the reconstruction of the head phantom along y=.017 line using weighted least square error filter of length 47.

filter to be large; but as the Fourier coefficients of the projection data is very small in this range, they do not produce significant reconstruction errors. Figure 4.8 shows reconstruction for a filter of length N= 35. Although Figure 4.8 shows higher reconstruction errors than in case of N=47, this reconstruction should be acceptable for many practical applications. Figure 4.9 shows the result of reconstruction using the same kind of filter with length N=31. This result shows increased deviation.

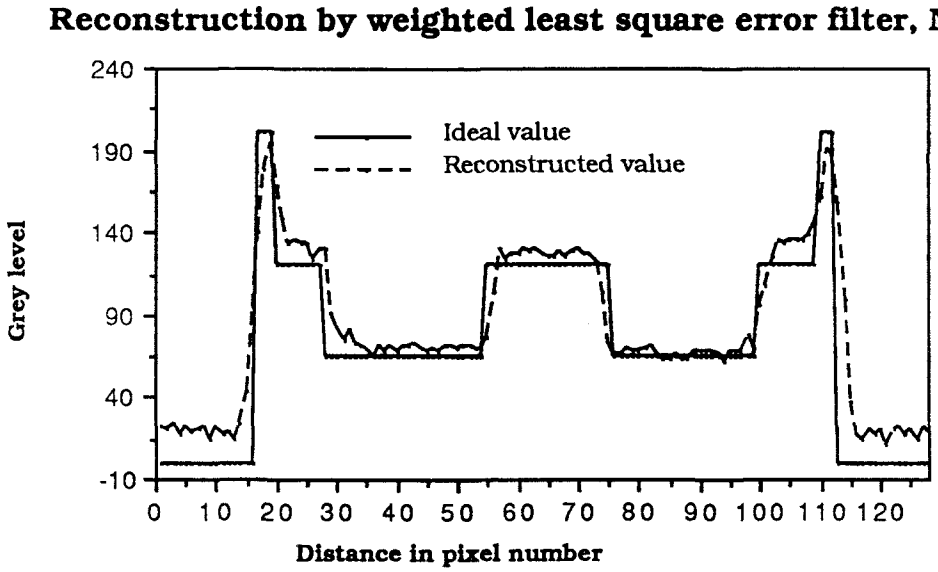

Fig 4.8: Comparison of the reconstruction of the head phantom along y=.017 line using weighted least square error filter of length 35.

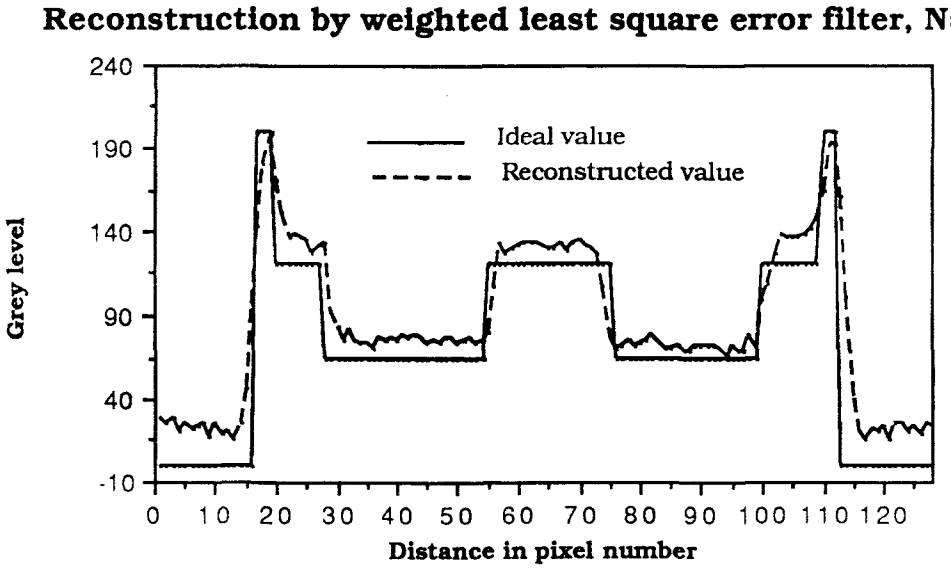

Fig 4.9: Comparison of the reconstruction of the head phantom along y=.017 line using weighted least square error filter of length 31.

Comparison of Performances: To compare the performances of the two kinds of filters discussed here, signal to noise ratio in the reconstructed images has been calculated. Signal to noise ratio has been defined as

$$SNR = 10 \log \frac{\sum_i \sum_j f(i,j)^2}{\sum_i \sum_j \{f(i,j) - g(i,j)\}^2}$$

where f(i,j) are the pixels of the ideal image and g(i,j) are the pixels of the reconstructed image. Figure 4.10 shows the variation of signal to noise ratio with the length of the filters. This figure indicates the better signal to noise ratios for the weighted least square error filters for given lengths.

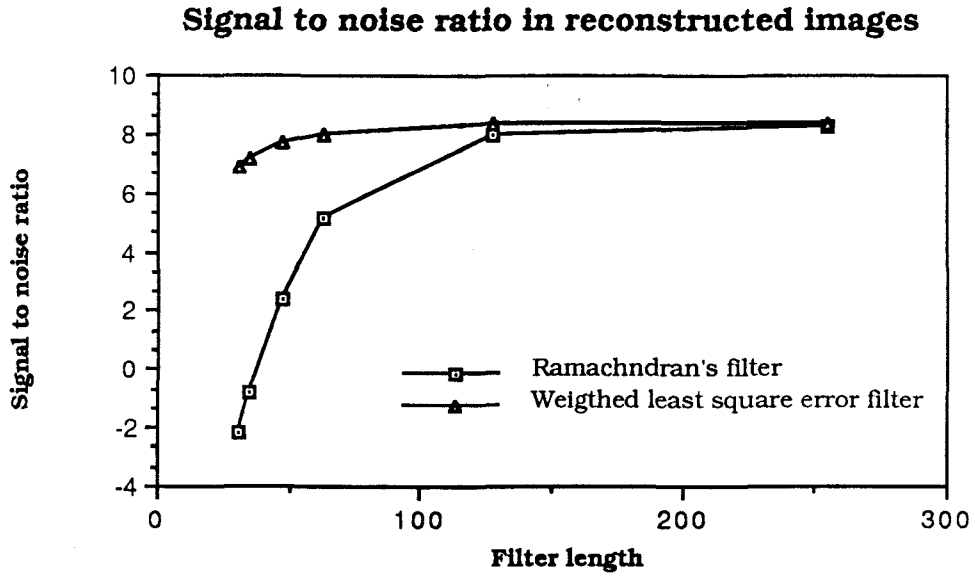

Fig 4.10: Signal to noise ratio in reconstructed images for the two kinds of filters.

CHAPTER V

SUMMARY AND CONCLUSIONS

Summary and Conclusions: The purpose of this thesis is to study the performance of least square error $|\omega|$ filters for image reconstruction from projections. The study evaluates the performance of the filters in reconstructing a simulated head phantom. Such a head phantom has been reported by other research workers to require high numerical accuracy and freedom of artifacts. The size of the reconstructed images are 128x128.

From the results presented in the previous chapter, it can be seen that the weighted least square $|\omega|$ filter performs better than the least square error filter suggested by Ramachandran for a given length. This conclusion is drawn from the results shown in Figure 4.10. This figure shows that the signal to noise ratio in reconstructed images are always higher for weighted least square error filters than for Ramachandran's filters for a given length.

For Ramachandran's filters, it can be seen that the reconstructed images for lengths N=255 and N=127 are of comparable accuracy. But after that the noise increases drastically as the length is shortened. One might find it easy to calculate the coefficients of Ramachandran's filter because of the associated analytic expressions.

Half of the coefficients of the Ramachandran's filter are zero. One may use this property to save computations in calculating the convolutions. So, when the signal to noise ratio of both the filters are of same order, as in the case of N=127, Ramachandran's filter may be preferable. On the other hand, the length of the weighted least square error filter can be reduced drastically for a very small decrease in signal to noise ratio; this slower rate of degradation of reconstruction can be realized from the slops of the two graphs in Figure 4.10.

Recommendation for Future Work: It can be mentioned here that there is another optimum filter design technique available which has been found very efficient in dealing with discontinuities of fuctions. This is known as the minimax approach and it minimizes the maximum approximation error. This approach can be tested for designing the $|\omega|$ filters.

Systolic array architectures have been found attractive for implementing convolution. Since convolution is a major part in the Convolution Backprojection method, another area of future research could be the implementation of this algorithm with systolic arrays.

BIBILOGRAPHY

[1] L. A. Shepp, B. F. Logan, "The Fourier Reconstruction of a Head Section", IEEE Trans, Nucl. Sci., Vol. NS-21, 1974, pp. 21-43.

[2] R. M. Lewitt, " Ultra Fast Convolution Approximation for Computerized Tomography", IEEE Trans, Nucl. Sci., Vol NS-26, No.2, April 1977, pp. 2678-2681.

[3] Y. S. Kwoh, I. S. Reed, T. K. Truong, " Backprojection Speed Improvement for 3-D Reconstruction", IEEE Trans, Nucl. Sci., Vol NS-24, No. 5, 1977, pp. 1999-2005.

[4] R. M. Reed, Y. S. Kwoh, T. K. Truong, E. L. Hall, "X-ray Reconstruction by Finite Field Transformations", IEEE Trans, Nucl. Sci., Vol. NS-24, 1977, pp. 843-849.

[5] L. S. Edelheit, G. T. Herman, A. V. Lakshminarayan, "Reconstruction of Objects from Diverging X-rays", Medical Physics 4, 1977, pp. 226-231.

[6] R. M. Lewitt, R. H. T. Bates, T. M. Peters, "Image Reconstruction from Projections: II: Modified Backprojection Methods", Optik 50, 1978, pp. 85-109.

[7] G. N. Ramachandran, A. V. Lakshminarayan, " Three Dimensional Reconstruction from Radiographs and Electron

Micrographs: Application of Convolution Instead of Fourier Transform", Proc. Nat. Acad. Sci., U. S. A., Vol 68, No. 9, 1971, pp. 2236-2240.

[8] R. M. Mersereau, " Direct Fourier Transform Techniques in 3-D Image Reconstruction", Comput. Biol. Med., Vol 6, 1976, pp. 247-258.

[9] W. E. Higgins, D. C. Munson, " A Hankel Transform Approach to Tomographic Image Reconstruction", IEEE Trans. Med. Imaging, Vol. 7, No. 1, 1988, pp. 59-71.

[10] A. Rosenfeld, A. C. Kak, "Digital Picture Processing", Second ed., Acaddemic press, 1982, Chapter 8.